Research Article | Vol. 29, No. 3 / 1 February 2021 / Optics Express 3524
Optics EXPRESS

All-dielectric orthogonal doublet cylindrical metalens in long-wave infrared regions

XIAOYAN SHI,[1,2] DEJIA MENG,[1] ZHENG QIN,[1,2] QIONG HE,[3] SHULIN SUN,[3] LEI ZHOU,[3] DAVID R. SMITH,[4,5] QING HUO LIU,[5] TARIK BOUROUINA,[6] AND ZHONGZHU LIANG[1,*]

[1]*State Key Laboratory of Applied Optics, Changchun Institute of Optics, Fine Mechanics and Physics, Chinese Academy of Sciences, Changchun, Jilin 130033, China*
[2]*University of the Chinese Academy of Sciences, Beijing 100049, China*
[3]*State Key Laboratory of Surface Physics, Key Laboratory of Micro and Nano Photonic Structures (Ministry of Education), and Department of Physics, Fudan University, Shanghai 200438, China*
[4]*Center for Metamaterials and Integrated Plasmonics, Duke University, Durham, NC 27708, USA*
[5]*Department of Electrical and Computer Engineering, Duke University, Durham, NC 27708, USA*
[6]*Electronique, Systèmes de Communications et Microsystèmes Lab, UMR 9007 Centre National de la Recherche Scientifique, Univ Gustave Eiffel, 77454 Marne-la-Vallée, France*
[*]*liangzz@ciomp.ac.cn*

Abstract: Metalens have been recently introduced to overcome shortcomings of traditional lenses and optical systems, such as large volume and complicated assembly. As a proof-of-principle demonstration, we design an all-dielectric converging cylindrical metalens (CML) for working in long-wave infrared regions around 9 μm, which is made up of silicon-pillar on MgF_2 dielectric layer. We further demonstrate the focusing effect of an orthogonal doublet cylindrical metalens (ODCM). Two CMLs are combined orthogonally and a circular focusing spot was demonstrated. This proves that within a certain size range, the focusing effect achieved by the ODCM is similar to that of a traditional circular metalens.

1. Introduction

The imaging effect of lenses has long been recognized and is routinely used in daily life, mainly in the visible spectral range. With the continuous development of science and technology, cylindrical lens as a simple alternative to spherical lens. Positive cylindrical lens have a converging effect on light and the combination of cylindrical lens and spherical lens can be widely used in fields such as laser beam expansion, eyewear optics, and wide-screen movie lenses. However, the cylindrical lens achieves a converging effect in only one direction, while the other direction does not converge the light beam, hence limiting their applications if not combined with other lenses. Regarding the traditional materials used for long-wave infrared lens, they are still classified into two major categories, crystals and glasses. Compared with the materials that can be used as visible optical lenses, the infrared materials with perfect physical and chemical properties are very limited. More importantly, the refractive index of infrared materials is generally high, which generally leads to low transmittance of infrared lenses. Then, because a complete optical system in long-wave infrared requires multiple traditional lenses, the energy loss of the whole system will be consequently too large. Therefore, it is necessary to control the number of lenses of the long-wave infrared system as much as possible. Furthermore, the processing technology of the long-wave infrared lens is also more complicated than for visible lens. All these factors have caused the long-wave infrared lens system to be expensive.

In recent years, due to the unique electromagnetic properties of subwavelength micro / nano structures, the polarization, phase, and amplitude of light waves can be flexibly manipulated. Therefore, metamaterials based on subwavelength micro / nano structures have developed rapidly

#414001 https://doi.org/10.1364/OE.414001
Journal © 2021 Received 4 Nov 2020; revised 20 Dec 2020; accepted 4 Jan 2021; published 21 Jan 2021

Optics EXPRESS

and achieved many extraordinary applications [1–5], such as high-dimensional holographic images [6–11], beam shaping [12], stealth cloaks [13], polarization control [14], and absorbers [15–18], sensing, etc. As an emerging technique, metalens is becoming one of the most popular directions of research on micro/nanostructured metasurfaces, as they enable controlling the wavefront of light. Based on its planar topography and strong ability to manipulate light waves, metalens has the advantages of ultra-light, ultra-thin, and easy integration. High NA metalens [19], achromatic metalens [20–23] have been realized. Metalens are expected to open a new path for sub-wavelength imaging and ultra-micro optoelectronic devices. However, large traditional circle metalens designs result into large amounts of data to process [24], and the extremely high data density over a certain area creates a total file size that becomes difficult to control due to the huge amount of geometrical features. Recently, research on metalens in the visible and near-infrared bands has been well developed, such as single-wavelength [19,24], multi-wavelength [21,25,26], and broadband achromatic metalens [27]. At present, the research on the meta-lens of the long-wave infrared band [20,23,27] is still limited by traditional materials used in long-wave infrared spectral range. However, this long-wave infrared spectral range is of great interest in thermal imaging and has great application prospects, which is the main motivation of our work. Transmissive metalens [28–31] is attracting increasing interest and could be an interesting option to achieve our goal. Therefore, the long-wave infrared metalens faces many challenges such as the limitation of traditional infrared materials.

In order to solve the above-mentioned problems of generating extremely high design data density when designing metasurfaces, and breaking the limitation of the materials used for long-wave infrared lens, we design an all-dielectric converging cylindrical metalens (CML) for working in long-wave infrared region around 9 μm wavelength. Since the CML focuses in only one direction, the amount of data will be greatly reduced and the array design only needs to be done in one direction. The simulation difficulty of cylindrical metalens is much smaller than that of a complete traditional metalens, and as the size increases, the data growth of a column structure is much slower. All-dielectric CMLs are made up of silicon nano column arrays on MgF_2 dielectric layer, which breaks through the material limitation of traditional long-wave infrared materials. The results show a high transmittance of 78.29%. Based on the CML, we design the ODCM which greatly reduces the difficulty of metalens design, too. The ODCM consists of two orthogonally CMLs, and allows obtaining a circular focusing spot with a transmittance of 52.43%. The intensity ratio of the focus center is 77.75%. Within a certain range, the focusing effect of the ODCM is similar to that of a traditional circular metalens of much more complex design features, but the ODCM greatly reducing the computational design difficulty of traditional metalens. For the cylindrical lens, the focusing effect of the designed cylindrical metalens can be obtained by designing and simulating a column of data results and then the column structure can be copied to obtain the array structure. The design data in this article is the simulation data volume of a column structure, which is much smaller than the design simulation data volume of a conventional metalens. When the design idea proposed in this paper is established, the amount of design data is only the amount of simulation data of two-column structure (orthogonal two-column structures). This design method of ODCM breaks through major limitations due to traditional materials used in long-wave infrared spectral range. It also greatly reduces the data amount of the traditional metalens design. In this work, in response to those major challenges, we have captured the characteristics of orthogonal doublet cylindrical lens, and reduced the amount of simulation data of traditional metalens, which greatly reduces the difficulty of metalens design.

2. CML structure design

Based on Huygens electromagnetic metasurface, we realize a metalens with a series of high transmittance and phase controllable dielectric artificial atoms. First of all, the design and material selection of the unit structure is significant. One cylindrical lens has a converging

Optics EXPRESS

or diverging effect in only one direction. The other direction acts as a flat glass and does not converge or diverge the ray, as shown in Fig. 1(a). We select Si as the material of the array structure. It is non-absorbing in the long-wave infrared region and its refractive index has a high contrast with the refractive index of the environment. Therefore, electromagnetic waves will be highly concentrated in the Si nano-cylinder. The phase shift can cover merely the whole range of 0-2π by changing the radius of the Si cylinders.

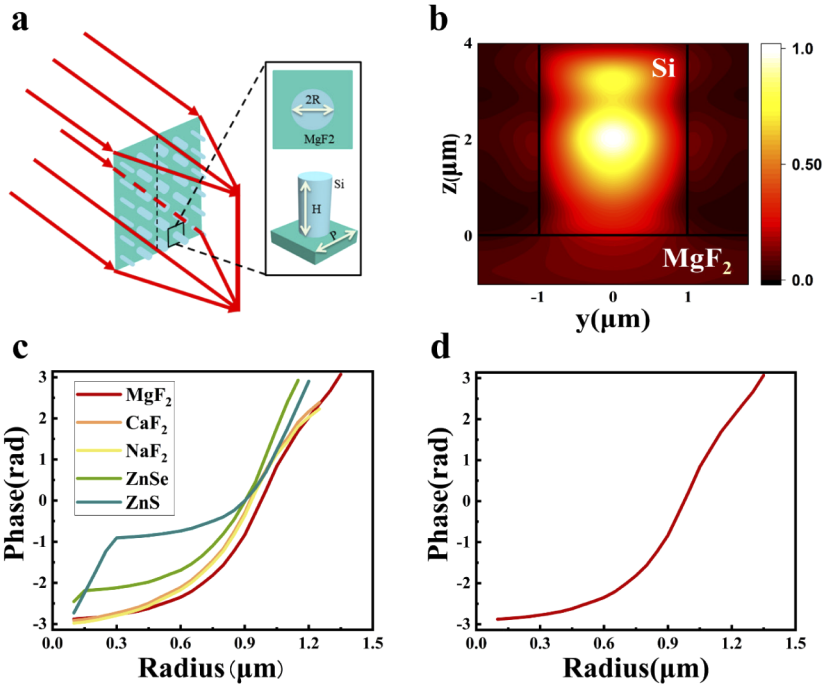

Fig. 1. Schematic diagram of the unit structure of metalens and the phase profile. (a) Schematic diagram of a positive cylindrical metalens, micro / nano unit structure, a square MgF_2 dielectric layer with a side length P = 3.6 μm, Si cylinder height h = 4 μm. And the incident wavelength is plane light of 9 μm. The permittivity of Si material is 3.4219. The refractive index of the Si coming from the data of the literature [32]. (b) Simulated xz-slices of normalized energy vector diagram of a single Si cylindrical structure supported by the MgF_2 dielectric layer. (c) When changing the base material, the phase profile changes with the radius of the Si cylinder. The larger the radius, the larger the phase delay. (d) The phase profile changes with the radius of the Si cylinder supported by the MgF_2 dielectric layer.

Secondly, we choose materials with high transmission in the long-wave infrared region as the dielectric layer of the all-dielectric metasurface. The simulation uses the finite difference time-domain (FDTD) algorithm for calculation. According to Fig. 1(b), we can find that the energy is concentrated in the Si cylinder, while it is relatively small in the dielectric layer. We made simulations with a series of materials having high transmission in the long-wave infrared range, as shown in Fig. 1(c). We decided to choose MgF_2 as the dielectric layer material for a better result of phase shift. We have determined the complete unit structure, as shown in Fig. 1(d). The Si cylinder is arranged on MgF_2 basement to modulate the phase of the incident light according to effective medium within the unit cell. At a wavelength of 9 μm, the phase shift covers the range of 0-2π with the change of radius of the Si cylinder ranging from 0.10 to 1.35 μm. Here, H is the designed Si nanopillar height (H = 4 μm), P is the period of unit cell (P = 3.6 μm), and its phase shift changes with the size of the nanopillar radius.

Optics EXPRESS

In transmission mode, in order to achieve convergence, the wavefront generated by the metasurface structure can be expressed by the following equation:

$$\Phi = \frac{2\pi}{\lambda}\left(f - \sqrt{f^2 + x^2 + y^2}\right) \tag{1}$$

Here, λ is the design wavelength (λ = 9 μm), f is the target focal length (f = 90 μm), x and y are position coordinates of each nanopillar with respect to an origin at the center of each lens. According to Eq. (1), the phase profile on the metalens is related to the design wavelength λ, the focal length f, and the location of each cell on the metalens.

A cylindrical lens has a converging or diverging effect in only one direction. The other direction acts as a flat glass and does not converge or diverge the ray. According to the characteristics of cylindrical lens, we can design just a row cylindrical structure to achieve the imaging effect. A positive cylindrical lens has a converging effect on light, which is the first focus of this work. Indeed, our aim is to design a CML first, which will then serve as a building block for the ODCM.

Taking y = 0, Eq. (1) leads to the following required phase profile:

$$\Phi_x = \frac{2\pi}{\lambda}\left(f - \sqrt{f^2 + x^2}\right) \tag{2}$$

When λ = 9 μm, f = 90 μm, the relationship between the phase profile required to realize the metalens and the position x on the lens. Upon wrapping, the phase is controlled in the 0-2π range as shown in Fig. 2(a). We split the design according to this cycle, and we select points at equal x intervals to get the position where we need to place the unit structure and its corresponding phase profile, as shown in the Fig. 2(a). Therefore, according to the relationship between the phase profile and the radius of the Si nanocylinder, an arrayed structure arranged on the MgF_2 dielectric layer can be obtained, as shown in Fig. 2(b).

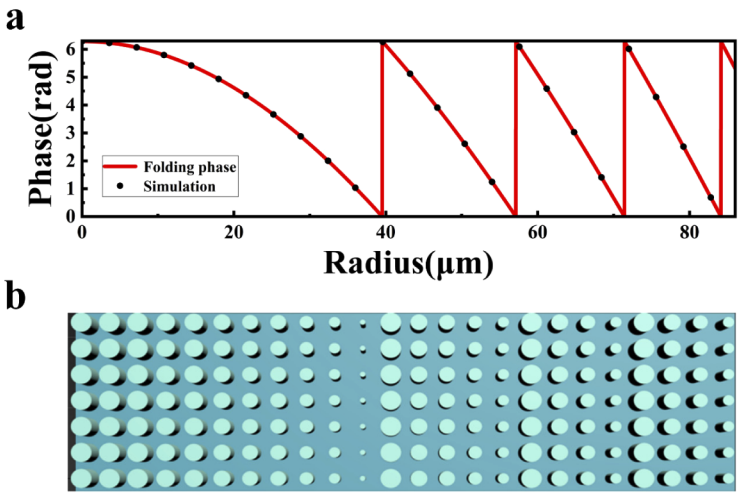

Fig. 2. Phase profile and array diagram. (a) The phase calculated by formula (2) is folded and controlled within the range of 0-2π from 0 to 86.5 μm, and take points at equal intervals according to the period of unit structure, P. (b) The top view (xy slices) of the array structure and the range is (0-86.5 μm). The radius of the Si cylinder in the x direction changes with position.

The incident light is selected to be a plane wave at 9 μm. When the total length of the simulation domain in the x-direction is 172.7 μm, the overall transmittance obtained is 78.29%,

Optics EXPRESS

and the strongest focusing is achieved at 99 μm back of the structure, as shown in the Fig. 3(a). The normalized intensity in the x-direction and the phase profile along the focal plane are shown in the Fig. 3(b). From the phase profile obtained from the simulation, we can find that its curve is not particularly smooth. It is mainly caused by discrete unit structure and periodic array arrangement. The analysis results show that the width at half the maximum intensity (FWHM) is 5.4 μm in the intensity curve. The focus center intensity ratio is 72.91%, and the convergent intensity is 57.08% of the incident light intensity.

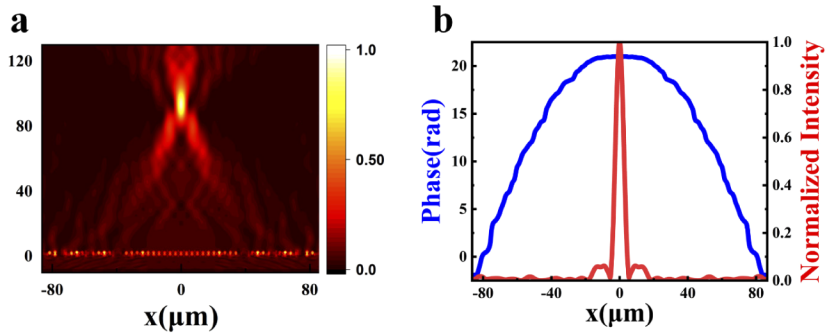

Fig. 3. (a) Normalized energy diagram on the x-z slices, focusing is achieved at 90-110 μm after the incidence of plane light. (b) Normalized intensity of x when z is chosen as 95 μm and y is chosen as 0, and the energy is concentrated in the center. The phase profile after the structure Orthogonal doublet cylindrical metalens.

3. Orthogonal doublet cylindrical metalens

According to the principles of geometric optics, it can be known that a cylindrical metalens CML has a converging effect in only one direction. We therefore combine two CMLs orthogonally and compare the corresponding result with those of a spherical lens. For this purpose, we arrange the two CMLs in the orthogonal directions on both sides of the same layer which serves as a common base medium to achieve the effect of an orthogonal doublet CMLs. As shown in Fig. 4(a), the two CML arrays are arranged in an orthogonal manner. The array above the dielectric layer controls the phase only in the x direction, while the array on the bottom layer only controls the phase only in the y direction. When the light passes through the two-layer array, phase control is carried out on the two directions to achieve focusing, when the incident ray is a plane wave as shown in Fig. 4(b). MgF_2 with the thickness of 1 μm, was selected as the dielectric layer in the middle connecting the two CMLs, and both corresponding cylindrical arrays are made of Si.

Without considering the thickness of the two orthogonal CMLs, the phase profiles of the CML of y direction can be obtained as:

$$\Phi_y = \frac{2\pi}{\lambda}\left(f - \sqrt{f^2 + y^2}\right) \tag{3}$$

Assuming that the focusing effect of two orthogonal CMLs is the same as that of a circular metalens, according to Eq. (2) and Eq. (3), we can obtain the equation,

$$\Phi = \Phi_x + \Phi_y \tag{4}$$

So, we can get

$$\frac{2\pi}{\lambda}\left(f - \sqrt{f^2 + x^2 + y^2}\right) = \frac{2\pi}{\lambda}\left(f - \sqrt{f^2 + x^2}\right) + \frac{2\pi}{\lambda}\left(f - \sqrt{f^2 + y^2}\right) \tag{5}$$

Optics EXPRESS

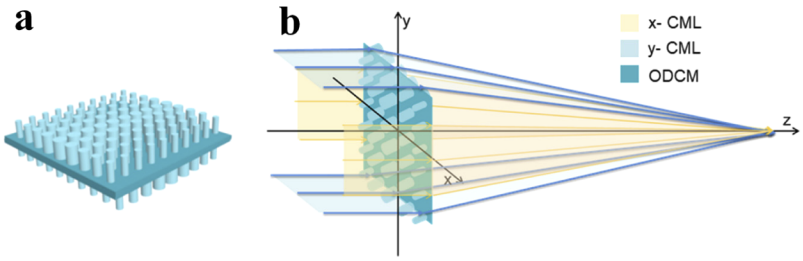

Fig. 4. (a) Schematic diagram of ODCM. The two CML arrays are arranged in an orthogonal manner. The array above the dielectric layer only controls the phase in the x direction, while the array on the bottom layer only controls the phase in the y direction. And MgF_2 was selected as the base material connected the two arrays, and the two cylindrical arrays are made of Si. (b) Schematic diagram of focusing of o ODCM. When the light passes through the two-layer array, phase control is carried out on the two directions to achieve focusing, when the incident ray is a plane wave.

To simplify Eq. (5) by exchanging and squaring the terms on both sides, it can be obtained the Eq. (6):

$$x^2 \cdot y^2 = 0 \tag{6}$$

So, when the maximum value of x^2y^2 is small enough, the above conditions can be met.

Based on the metalens presented in this paper, we have placed two CMLs, both with a focal length of f = 90 μm in orthogonal arrangement, and discussed the range in which they can achieve a focal spot similar to a circular metalens. First, we selected three groups of ODCM with the different width for simulation. The length of side of the three groups were D = 100μm, D = 197μm, and D = 361μm at the same wavelength of 9 μm. The resulting focusing effects are shown in Fig. 5. As shown in Fig. 5, we can see that the focus on the xz and yz planes is slightly different. The main reason is that the arrays for phase control in two directions are on both sides of the dielectric layer. From the focus distance, the focus position is slightly deviated, which leads to this phenomenon.

For those different ODCMs, we obtain three sets of the energy vector diagrams, shown along two orthogonal propagation surfaces (x-z, y-z), and the energy vector diagrams of x-y surface where the energy is most concentrated in the direction of propagation. That is, when z is constant and y = 0 μm, the linear normalized intensity graph of energy is changing with the x position. The peak range of energy concentration is selected to calculate the focusing efficiency. From this, we find that ODCM with a size of D = 100 μm has the strongest focus at 88 μm behind the lens. The corresponding FWHM of focal spot is 8.92 μm, the intensity ratio of the focus center region is 77.75%, and the metalens transmittance is 61.7%. Therefore, the focusing efficiency of ODCM is 47.97% and the NA is 0.494. The ODCM with a size D = 197 μm has the strongest focus at 85 μm behind it. The corresponding FWHM is 5.4 μm, the intensity ratio of the focus center region is 80%, and the metalens transmittance is 52.85%. Therefore, the focusing efficiency of ODCM is 42.28% and the NA is 0.757. The ODCM with a size of D = 361 μm has the strongest focus at 85 μm behind it with a high NA of 0.905. The corresponding FWHM is 5.23 μm, the intensity ratio of the focus center region is 52.92%, and the metalens transmittance is 41%. Therefore, the focusing efficiency of ODCM is 21.7% and the NA is 0.905.

Comparing those three groups of ODCMs, we can find that the ODCM with the size of 100 μm (D = 100μm) has a slightly dispersed focus with sub-focus points along the light propagation direction, and the focus spots are more rounded. In the meantime, the energy intensity of the main focus point is high. In the ODCM with size of 197 μm, the focus spot is closest to a circle, and it does not have a sub-focus point in the propagation direction. Also, in the ODCM

Optics EXPRESS

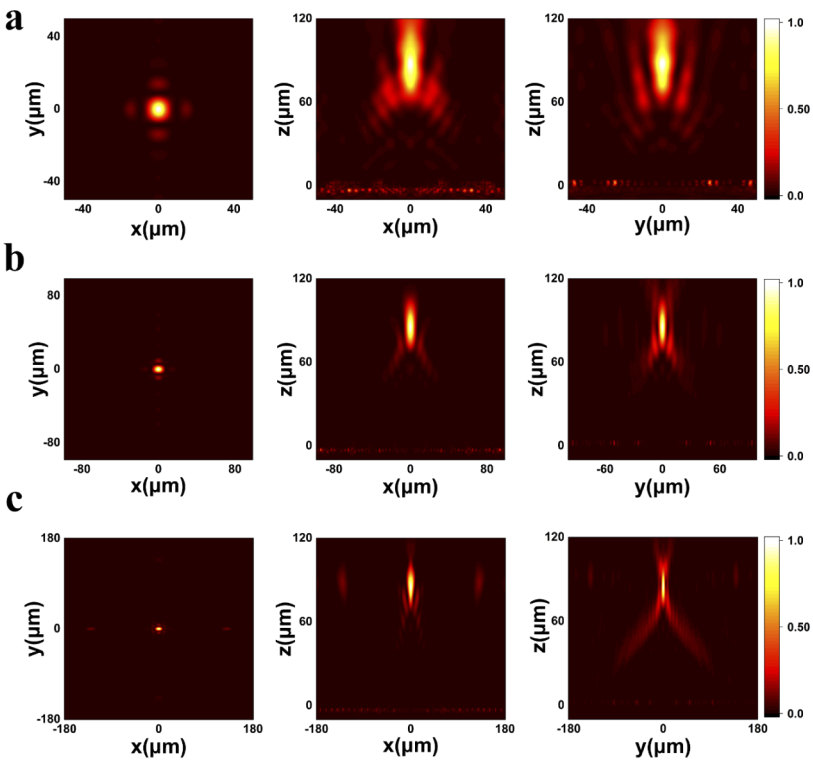

Fig. 5. Normalized energy diagram of the focal spot at three different wavelength, λ = 8.8, 8.9, 9.0 μm. In the 0.2 μm wavelength region, the focus center position is basically uniform.

with size of 361 μm, there is no sub-focusing concentration point in the propagation direction, but the transmission is low. And it has a focus center spot in the shape of a cross. Figure 6 show the normalized intensity along x with ODCM lateral size of 100 μm (197 μm, 361 μm) respectively, and the energy is concentrated in the center. The focus, transmittance, focusing efficiency, FWHM and Numerical aperture (NA) of the three ODCM with different size lengths are shown in Table 1.

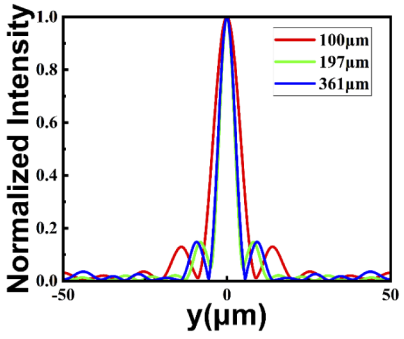

Fig. 6. Normalized intensity along with x with size of 100 μm (197μm, 361μm) and the energy is all concentrated in the center.

After comparing the focusing effects of three groups of ODCM of different sizes, the focusing effect achieved by the ODCM is similar to that of a circular metalens within a certain range.

Optics EXPRESS

Table 1. Focus, transmittance, focusing efficiency, FWHM and Numerical aperture (NA) of the ODCMs with different size lengths.

Side length (μm)	Focus (μm)	Transmittance (%)	Focusing efficiency (%)	FWHM (μm)	Numerical aperture (NA)
100	88	61.7	47.97	8.92	0.494
197	85	52.85	42.28	5.4	0.757
361	85	41	21.7	5.23	0.905

Since the CML focuses in only one direction, the amount of data will be greatly reduced and the array design only needs to be done in one direction, in other words, we just need to design a row cylindrical structure. The simulation difficulty of a column array is much smaller than that of a complete metalens, and as the size increases, the data growth of a column structure is much slower. We reduce the amount of data in the design of the metalens by designing the relevant CML. We can design a CML and then orthogonally design it to achieve the focusing effect, which greatly reduces the difficulty of metalens design.

4. Conclusions

Based on the theory of plasmonic and micro-nano processing technology, we study the mechanism of phase adjustment through dielectric metasurfaces, leading to the designs and simulation of a metasurface structure that achieves phase control of light. By designing the micro / nano structure array, we obtained the parameter properties of the phase profile changed with the geometric parameters of the Si cylinder supported by an MgF_2 dielectric layer. Based on the phase profile properties, a CML operating at a wavelength of 9 μm was designed with a focusing efficiency of 57.08%. Then, on the basis of this CML, an ODCM was further designed and simulated in three different lateral dimensions D. When the size of the ODCM is 100 μm, the focusing efficiency reaches 47.97% with the NA of 0.494. Based on the above results, it is shown that within a certain size range, an ODCM can achieve focused spots. It breaks through the limitation of natural infrared materials, opening a pathway towards flat lenses operating in the long-wavelength infrared, achievable by reasonable design, which improves the performance of the long-wave infrared metalens from the principle and material basis. The ODCM greatly reduces the difficulty of designing conventional metalens by reducing the amount of simulation data required by the design. The long-wave infrared-based ODCM has a wide range of applications, and has many advantages such as small size and light weight. It will be used in infrared imaging detection, sensing, spectral analysis, temperature detection, meta-resolution imaging and other fields.

Funding. National Natural Science Foundation of China (61735018, 61805242, 61376122); Leading Talents and Team Project of Scientific and Technological Innovation for Young and Middle-aged Groups in Jilin Province (20190101012JH); Jilin Scientific and Technological Development Program (20170204077GX, 20190103014JH); Youth Innovation Promotion Association of the Chinese Academy of Sciences (2014193, Y201836); Project of CIOMP-Fudan University Collaborative Research; Independent fund of State Kay Laboratory of Applied Optics; Project of CIOMP-Duke Collaborative Research (201903002); Overseas Students Science and Technology Innovation and Entrepreneurship Projects.

Disclosures. The authors declare no conflicts of interest.

References

1. I. Barth, D. Conteduca, C. Reardon, S. Johnson, and T. F. Krauss, "Common-path interferometric label-free protein sensing with resonant dielectric nanostructures," Light: Sci. Appl. **9**(1), 96 (2020).
2. A. C. Overvig, S. Shrestha, S. C. Malek, M. Lu, A. Stein, C. Zheng, and N. Yu, "Dielectric metasurfaces for complete and independent control of the optical amplitude and phase," Light: Sci. Appl. **8**(1), 92 (2019).
3. A. A. Sergeev, D. V. Pavlov, A. A. Kuchmizhak, M. V. Lapine, W. K. Yiu, Y. Dong, N. Ke, S. Juodkazis, N. Zhao, S. V. Kershaw, and A. L. Rogach, "Tailoring spontaneous infrared emission of HgTe quantum dots with laser-printed plasmonic arrays," Light: Sci. Appl. **9**(1), 16 (2020).

Optics EXPRESS

4. D. Zhang, L. Lan, Y. Bai, H. Majeed, M. E. Kandel, G. Popescu, and J. X. Cheng, "Bond-selective transient phase imaging via sensing of the infrared photothermal effect," Light: Sci. Appl. **8**(1), 116 (2019).
5. S. Shrestha, A. C. Overvig, M. Lu, A. Stein, and N. Yu, "Broadband achromatic dielectric metalenses," Light: Sci. Appl. **7**(1), 85 (2018).
6. D. Wen, F. Yue, G. Li, G. Zheng, K. Chan, S. Chen, M. Chen, K. Li, W. Wong, K. Cheah, E. Pun, S. Zhang, and X. Chen, "Helicity multiplexed broadband metasurface holograms," Nat. Commun. **6**(1), 8241 (2015).
7. L. Huang, H. Mühlenbernd, X. Li, X. Song, B. Bai, Y. Wang, and T. Zentgraf, "Broadband Hybrid Holographic Multiplexing with Geometric Metasurfaces," Adv. Mater. **27**(41), 6444–6449 (2015).
8. Y.-W. Huang, W. Chen, W.-Y. Tsai, P. Wu, C.-M. Wang, G. Sun, and D. P. Tsai, "Aluminum Plasmonic Multicolor Meta-Hologram," Nano Lett. **15**(5), 3122–3127 (2015).
9. L. Wang, S. Kruk, H. Tang, T. Li, I. Kravchenko, D. N. Neshev, and Y. S. Kivshar, "Grayscale transparent metasurface holograms," Optica **3**(12), 1504–1505 (2016).
10. W. T. Chen, K.-Y. Yang, C.-M. Wang, Y.-W. Huang, G. Sun, I. D. Chiang, C. Y. Liao, W.-L. Hsu, H. T. Lin, S. Sun, L. Zhou, A. Q. Liu, and D. P. Tsai, "High-Efficiency Broadband Meta-Hologram with Polarization-Controlled Dual Images," Nano Lett. **14**(1), 225–230 (2014).
11. K. Huang, Z. Dong, S. Mei, L. Zhang, Y. Liu, H. Liu, H. Zhu, J. Teng, B. Luk'yanchuk, J. K. W. Yang, and C.-W. Qiu, "Silicon multi-meta-holograms for the broadband visible light," Laser Photonics Rev. **10**(3), 500–509 (2016).
12. B. Zeng, Z. Huang, A. Singh, Y. Yao, A. K. Azad, A. D. Mohite, A. J. Taylor, D. R. Smith, and H. T. Chen, "Hybrid graphene metasurfaces for high-speed mid-infrared light modulation and single-pixel imaging," Light: Sci. Appl. **7**(1), 51 (2018).
13. X. Ni, Z. Wong, M. Mrejen, Y. Wang, and X. Zhang, "An ultrathin invisibility skin cloak for visible light," Science **349**(6254), 1310–1314 (2015).
14. M. Khorasaninejad, W. Zhu, and K. Crozier, "Efficient polarization beam splitter pixels based on a dielectric metasurface," Optica **2**(4), 376 (2015).
15. W. Chen, R. Chen, Y. Zhou, and Y. Ma, "Broadband metamaterial absorber with an in-band metasurface function," Opt. Lett. **44**(5), 1076–1079 (2019).
16. S. Wang, C. Cai, M. You, F. Liu, M. Wu, S. Li, H. Bao, L. Kang, and D. H. Werner, "Vanadium dioxide based broadband THz metamaterial absorbers with high tunability: simulation study," Opt. Express **27**(14), 19436–19447 (2019).
17. X. Zhao, C. Chen, A. Li, G. Duan, and X. Zhang, "Implementing infrared metamaterial perfect absorbers using dispersive dielectric spacers," Opt. Express **27**(2), 1727–1739 (2019).
18. S. Fardad and A. Salandrino, "Plasmonic parametric absorbers," Opt. Lett. **43**(24), 6013–6016 (2018).
19. R. Paniagua-Domínguez, Y. F. Yu, E. Khaidarov, S. Choi, V. Leong, R. M. Bakker, X. Liang, Y. H. Fu, V. Valuckas, L. A. Krivitsky, and A. I. Kuznetsov, "A Metalens with a Near-Unity Numerical Aperture," Nano Lett. **18**(3), 2124–2132 (2018).
20. D. Tang, C. Wang, Z. Zhao, Y. Wang, M. Pu, X. Li, P. Gao, and X. Luo, "Ultrabroadband superoscillatory lens composed by plasmonic metasurfaces for subdiffraction light focusing," Laser Photonics Rev. **9**(6), 713–719 (2015).
21. O. Avayu, E. Almeida, Y. Prior, and T. Ellenbogen, "Composite functional metasurfaces for multispectral achromatic optics," Nat. Commun. **8**(1), 14992 (2017).
22. S. Wang, P. C. Wu, V.-C. Su, Y.-C. Lai, C. Hung Chu, J.-W. Chen, S.-H. Lu, J. Chen, B. Xu, C.-H. Kuan, T. Li, S. Zhu, and D. P. Tsai, "Broadband achromatic optical metasurface devices," Nat. Commun. **8**(1), 187 (2017).
23. W. T. Chen, A. Y. Zhu, V. Sanjeev, M. Khorasaninejad, Z. Shi, E. Lee, and F. Capasso, "A broadband achromatic metalens for focusing and imaging in the visible," Nat. Nanotechnol. **13**(3), 220–226 (2018).
24. A. She, S. Zhang, S. Shian, D. R. Clarke, and F. Capasso, "Large area metalenses: design, characterization, and mass manufacturing," Opt. Express **26**(2), 1573–1585 (2018).
25. M. Khorasaninejad, W. Chen, R. Devlin, J. Oh, A. Zhu, and F. Capasso, "Metalenses at visible wavelengths: Diffraction-limited focusing and subwavelength resolution imaging," Science **352**(6290), 1190–1194 (2016).
26. M. Khorasaninejad, A. Y. Zhu, C. Roques-Carmes, W. T. Chen, J. Oh, I. Mishra, R. C. Devlin, and F. Capasso, "Polarization-Insensitive Metalenses at Visible Wavelengths," Nano Lett. **16**(11), 7229–7234 (2016).
27. M. Liu, Q. Fan, L. Yu, and T. Xu, "Polarization-independent infrared micro-lens array based on all-silicon metasurfaces," Opt. Express **27**(8), 10738–10744 (2019).
28. H. Huang, M. Zhao, X. Chen, S. Zhu, J. Tang, and A. Zhang, "Design and measurement-based characterization of a K-band metalens for wideband oblique-incident spherical-plane wave conversion," Int. J. RF Microw. Comp. Eng. **30**(2), e22055 (2020).
29. C. He, T. Sun, J. Guo, M. Cao, J. Xia, J. Hu, Y. Yan, and C. Wang, "Chiral Metalens of Circular Polarization Dichroism with Helical Surface Arrays in Mid-Infrared Region," Adv. Opt. Mater. **7**(24), 1901129 (2019).
30. S. Gao, C. S. Park, C. Zhou, S. S. Lee, and D. Y. Choi, "Twofold Polarization-Selective All-Dielectric Trifoci Metalens for Linearly Polarized Visible Light," Adv. Opt. Mater. **7**(21), 1900883 (2019).
31. K. Cheng, Z. Wei, Y. Fan, X. Zhang, C. Wu, and H. Li, "Realizing Broadband Transparency via Manipulating the Hybrid Coupling Modes in Metasurfaces for High-Efficiency Metalens," Adv. Opt. Mater. **7**(15), 1900016 (2019).
32. E. D. Palik, *Handbook of Optical Constants of Solids* (Academic Press, New York, 1985).